Chapter 4

THz QCLs Design Toward Real Applications

Tsung-Tse Lin

Additional information is available at the end of the chapter

http://dx.doi.org/10.5772/65351

Abstract

For highly desired THz applications, we discuss the design and fabrication of THz quantum cascade lasers (QCLs) toward the high temperature and large average output power operations for the real applications with the relatively compact portable size cryogenic cooling systems. We describe the temperature performance parameters of THz QCLs and introduce the recent results of an indirect injection design scheme in the THz region and modulation height active structure design with different barriers and wells for the further design direction. The recent fabricated THz QCLs are combined with the liquid nitrogen (LN) cooling Dewar condenser to demonstrate the relatively compact THz source unit by QCLs. The different injection schemes in THz and barriers-wells height design in the active region introduce one of the directions for the further high temperature and large output power operation of THz QCLs. The relatively compact size THz source unit with a cryogenic system demonstrates the THz QCLs for real applications with the milliwatt order average output operation near liquid nitrogen temperature.

Keywords: Terahertz, quantum cascade laser, semiconductor THz source

1. Introduction

The terahertz (THz) region in the electromagnetic spectrum has drawn much attention due to its wide range of applications in various fields such as spectroscopy, imaging, remote sensing, and communications. Compact THz semiconductor sources are also extremely promising for use in future high-speed and large-capacity local telecommunications applications, especially for those applications operating in the range from sub-THz to a few THz (0.2–2 THz) [1]. The output power of conventional mature radio frequency (RF) electronic devices reduces by 4 orders of magnitude with frequency, which is close to 1 THz in the order of a few microwatts (μW).

High-output-power continuous-wave (CW) operation of optical semiconductor devices is very attractive for overcoming this problem. Quantum cascade lasers (QCLs) [2] are compact semiconductor light sources that utilize carrier recycling and intersubband transitions in repeating quantum well (QW) structures, and they have been demonstrated to operate successfully in the mid-infrared (mid-IR) [2] and THz [3] regions. They are also arguably the only THz solid-state sources with average optical output power levels much greater than one milliwatt (mW). This property of high optical output power with a narrow emission line width is quite attractive for a wide range of THz applications.

The current status of THz QCLs that operate without an external magnetic field has been reported in the spectral range from 1.2 to 5.2 THz [4, 5] with a maximum output power of around 1.01 W in pulsed mode [6]. In contrast to the room temperature operation of mid-IR QCLs, the maximum operating temperature (T_{max}) of THz QCLs is 199.5 K [7] at 3.2 THz. This performance was realized by an optimized state-of-the-art $Al_{0.15}Ga_{0.85}As/GaAs$ structure utilizing longitudinal optical (LO) phonon depopulation for the extraction scheme with resonant tunneling (RT) injection and diagonal emission. However, even this temperature performance still limits their practical use in some applications. Higher operating temperatures for THz QCLs with wider frequency that can at least function at temperatures attainable using Peltier coolers (230–250 K) have been one of the most important topics in recent research. The commonly reported high-temperature performance of THz QCLs roughly follows an empirical limitation depending on their operating frequency, such that $T_{max} \sim h\omega/k_B$. Compared with the near 200 K operation of THz QCLs at 3–4 THz, at low frequencies (<2 THz), THz QCLs are expected to exhibit poorer temperature performance due to this limitation when the frequency decreases. THz QCLs that operate at low frequencies suffer from design difficulties due to the narrow radiative energy separation between the two lasing-subband levels, which is related to the narrow dynamic range of the current density of the laser. Large thermal perturbation effects within the narrow energy level spaces have prevented the expansion of THz QCLs to low-frequency high-temperature operation. This reduction in the dynamic range of the current density with operating frequency can be qualitatively explained by the dependence of RT injection scheme THz QCLs on $k_B T_{max} \sim h\omega$ [8]. It is known to be difficult to achieve both low-frequency lasing and high-temperature operation.

On the basis of some successful solutions in mid-infrared QCLs, the different barrier height shows some solution to improve the device performance for different directions. For example, utilizing the height barriers to reduce the high temperature parasitic leakage currents [9, 10] and step wells for improving internal quantum efficiencies [11]. Furthermore, with the high technique of crystal growth, the optimization of the individual barrier and well's height at the suitable place is possible to give the solution and one more design freedom of recent stagnated structure design of THz QCLs. Considering these research and our previous studies on high Al composition $Al_xGa_{1\_x}As/GaAs$ design [9], it indicates one of the possible directions for combining the high Al composition structure with variable well-barrier height design [12] in order to achieve the thermoelectric cooling and higher temperature operation of THz QCLs. For this kind of modulation well-barrier height modulation height active structure. It is also expected to utilize the further indirect injection design.

The recent two methods are introduced for improving the performance of THz QCLs. We demonstrate a relative compact-size semiconductor THz source unit by the recent fabrication of THz QCL devices for real applications. The operation temperature largely limited the real compact size potable THz applications by semiconductor-based QCLs. A compromise solution is to capitalize on the liquid nitrogen (LN_2) cooling Dewar condenser, keep the useful characteristics of THz QCLs and reduce the cooling system size, and realize the robust portable compact size THz source unit by QCLs. The output power is one of the most important characteristics required for the different real THz applications. The recently large peak output power THz QCLs are realized by a large size mesa with a semi-insulated surface plasmon (SI-SP) waveguide and achieved the 1 W peak power. But this still limited on the pulse operation, the average output of THz QCLs still recorded by the previous report [13]. Here, we introduce a Dewar condenser cooling system with our recent fabricated metal-metal waveguide (MMW) modulation height active structure THz QCLs and the premier measurement results of few microwatts average power with milliwatt order peak power, larger output power THz QCLs with the peak output power of 250 mW and the average output power of 2.2 mW, indicating the further improvement in the direction of the continuous-wave (CW) mW order average power operation. In the following paragraphs, we introduce the details of indirect injection low frequency THz QCLs, modulation height active structure design, and a Dewar condenser type THz source unit by THz QCLs.

2. Indirect injection THz QCLs for low frequency high T operation

An indirect injection scheme was first reported for mid-IR QCLs among the different kinds of injection schemes [14]. Illustrative band diagrams of typical resonant tunneling injection schemes are shown in **Figure 1**: (a) for a simplified three-level system and (b) for a simplified four-level indirect scattering-assisted injection scheme with diagonal THz emission, which is used in this work. Improvements in performance have been successfully achieved using fast and smooth LO phonon injection without carrier accumulation. This injection scheme is also expected to circumvent the limitations of the RT injection scheme and to enable the realization of low-frequency THz QCLs operating at high temperatures. However, the much larger radiative energy in the mid-IR region causes different subband transport characteristics that need to be considered in designs for THz frequencies. It is difficult to implement an indirect injection design with the correct carrier injection and narrow radiative energy at THz frequencies. Even this design scheme still suffers difficulties in the THz region compared with mid-IR QCLs. After several theoretical proposals [15–17], a few recent experimental reports [8, 18–20] of indirect injection designs show promising results and demonstrate that there is high potential for attaining low-frequency, high-temperature THz QCLs.

Here, we demonstrate an $Al_{0.175}Ga_{0.825}As/GaAs$ QCL design that uses a combination of indirect injection and a less vertical diagonal for emission in the THz region. Structures were grown on semi-insulating GaAs (100) substrates by solid-source molecular beam epitaxy (MBE). The growth sequence started with a 250-nm-thick $Al_{0.6}Ga_{0.4}As$ etch-stop layer. The active/injection layers, which are sandwiched between two 100-nm-thick *n*-GaAs layers ($n = 5.0 \times 10^{18}$ cm^{-3}),

are repeated 185 times with thicknesses of **3.95**/7.99/**2.16**/9.02/**3.19**/6.86/**3.76**/*14.38* (nm), and with $n = 2.1 \times 10^{16}$ cm^{-3} modulation doping employed for the widest well. After MBE growth, the wafers were processed into Cu-Cu MMW by Au-Au thermo compression wafer bonding. The 170 μm-wide ridges of the laser bars were fabricated using photolithography and Cl_2 dry etching. Finally, we cleaved the laser bars with a cavity length of 1.5 mm and measured them using a cryogenic Si-bolometer with an FT-IR system in pulsed mode. The emission spectrum is measured at 5 K and lasing is at 7.85 meV, corresponding to a frequency of 1.89 THz (wavelength of 158 μm). The observed emission energy was a little higher than the designed energy, possibly due to the grown layers being 0.5% thinner and the measured large operating voltage due to the decrease in voltage at the Schottky contacts on either side of the metal-metal waveguides. The current density-light output characteristics (*I-L* curve) and the current density-voltage characteristics (*I-V* curve) of this 1.9 THz $Al_{0.175}Ga_{0.825}As$/GaAs QCLs indicate that the *J*th at low temperature is about 700 A/cm^2 with an output peak power in the range of a few milliwatts, which was calibrated from the measurements conducted by using the Si-bolometer. In the low output range near the laser threshold, our *I-L* curve shows large noise during the measurement. This might be due to the experimental setup and the very low duty cycle (0.02%) pulse measurement. This THz QCL operated up to 160 K at a frequency of 1.9 THz, which is 1.8 times higher than the empirical temperature-frequency limitation of the conventional RT injection scheme.

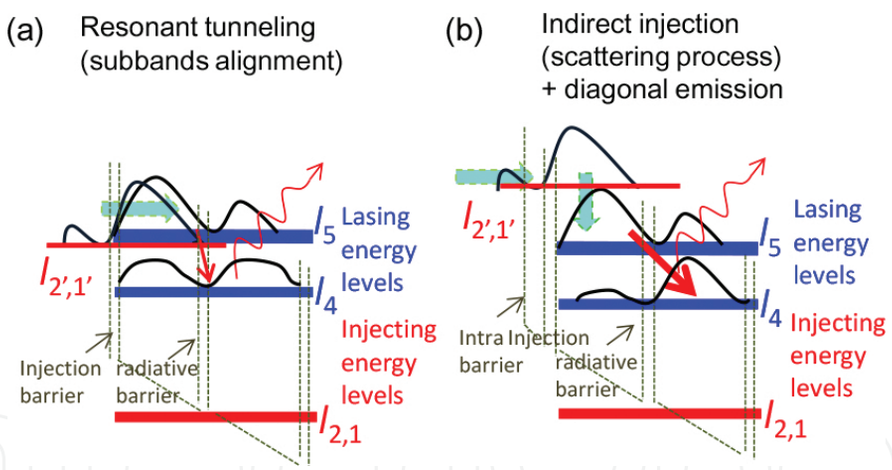

Figure 1. Illustrative band diagrams of (a) resonant tunneling injection scheme with subband alignment and (b) indirect scattering-assisted injection scheme with diagonal THz emission.

In practice, this kind of simplified four-level indirect injection scheme depends mainly on the external electrical field. **Figure 2** shows the dependence of the energy separation of the subbands on the external electric field for our structure. In the low electric field region around 12–14 kV/cm, the energy separation and band-diagram conditions are similar to the conventional RT injection scheme, as shown in **Figure 3(a)**: it shows a simplified three-level-type design including two lasing levels and one injection level with a subband alignment injection process; the band diagram related to this is shown in **Figure 1(a)**. The injection process occurs from $l_{2'}$ (the injection level at low bias) to $l_{1'}$ (the upper lasing level at low bias) via an RT injection

process. The emission frequency of about 5.0 THz (~20 meV) between $l_{1'}$ and l_5 (lower lasing level at low bias) is similar to the conventional RT injection lasing conditions. The first reported indirect type scattering-assisted (SA) injection QCLs in the THz region [8] also, initially, exhibited lasing at 4 THz. This emission occurred between similar subbands, $l_{1'}$ and l_5, to those in the RT injection scheme. When the external electric field is increased, the mechanism between $l_{1'}$ and l_5 changes from a radiative process to an injection process by fast nonradiative thermally activated LO phonon scattering. At higher electric fields, an LO phonon scattering process injects carriers and assists the targeted depopulation between l_5 and l_4 for emission at 1.8 THz. Here, our design optimizes the energy separation between $l_{2',1'}$ and l_5, increasing it in order to approach the designed LO phonon energy. The fast nonradiative-injection scattering process between $l_{2',1'}$, and l_5 occurs earlier and restricts the low electric field emission to 4–5 THz. We also carefully optimized the wavefunctions between l_1 and l_5, so that there is less overlap at low electric fields, with the related small oscillator strength reducing the possibility of lasing.

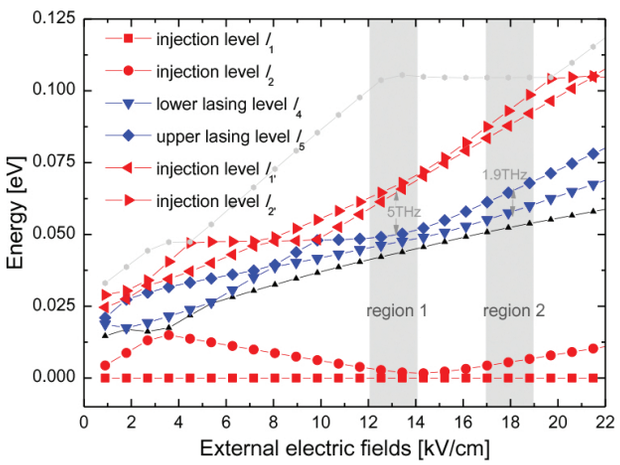

Figure 2. Calculated energies of the subband levels in the band diagram of the designed structure with respect to the external electric field. Region 1 is similar to conventional THz QCLs using the RT injection scheme, with a radiative energy of around 5 THz. Region 2 is for the indirect injection scheme combined with diagonal emission with a radiative energy below 2 THz.

We focus only on the realization of a radiative process at high electric fields for 1.9 THz lasing. This occurs in the range of 17–19 kV/cm, as shown in **Figure 2**, which is related to the designed band diagram presented in **Figure 3(b)**. Here, we utilize the LO phonon scattering process to selectively inject carriers from previous injection/extraction levels ($l_{2'}$, $_{1'}$) to the upper lasing level (l_5) indirectly. Then the LO phonon depopulation scheme extracts the carriers by fast LO phonon scattering from the lower lasing level (l_4) to the injection level ($l_{2,1}$) and injects the carriers into the next period of the cascade in order to achieve population inversion within l_5 and l_4. We calculated the relationship between the injection selectivity and the overlap between the wavefunctions of l_5 and l_4; as the spatial separation between the wavefunctions increases, the THz radiation changes from vertical to more diagonal. The indirect injection selectivity from the injection level to the two lasing levels improves. As the overlap of the $l_{2',\,1'}$ and l_4 wavefunctions gets smaller, the unwanted parasitic leakage channel between $l_{2',1'}$ and l_4 is

reduced. As calculated, if the LO-phonon scattering relaxation time from $l_{2',1'}$ to l_5 is kept near 0.7 ps, and the wavefunction overlap ratio of $f(l_{2',1'}, l_4)/f(l_{2',1'}, l_5)$ is changed from 0.9 (large overlap of l_5 and l_4) to 0.18 (small overlap of l_5 and l_4 used in this design), then the emission of l_5 to l_4 changes from vertical to diagonal. The relaxation time for the parasitic injection scattering from $l_{2',1'}$ to l_4 increases from 0.8 to 4 ps. It estimates the improvement of injection selectivity by increasing radiation diagonal and realizes this indirect injection scheme in THz QCLs. In our previous work, we demonstrated that the use of AlGaAs with a high Al content in a THz QCL [21] brings some advantages for high temperature operation. This high-Al content barrier structure provides the benefit of having high conduction-band offsets with spatially separated wavefunctions. We prefer to use thin high-Al content AlGaAs barriers or different barrier height active structures (it will describe in detail in the next paragraph) in order to achieve an indirect injection scheme at THz frequencies with better injection selectivity by utilizing the diagonal emission design.

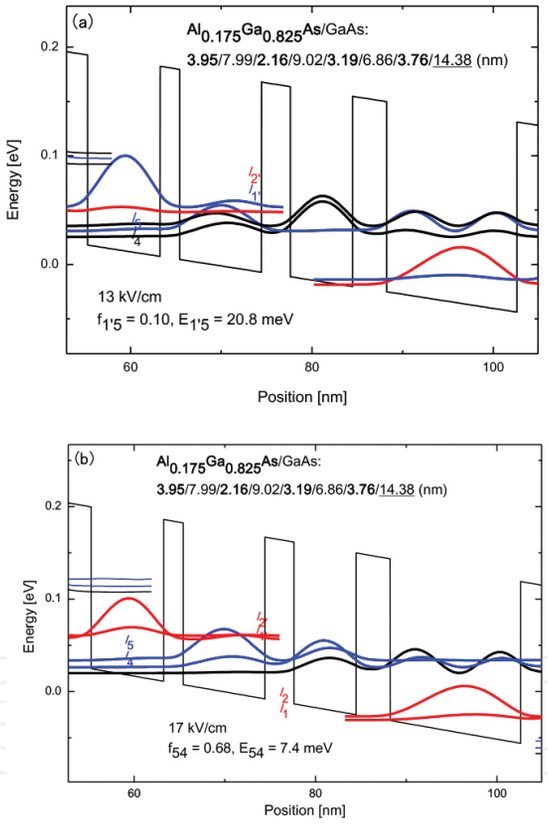

Figure 3. Self-consistent calculations of the conduction band diagrams of the **$Al_{0.175}Ga_{0.825}As$**/GaAs THz QCLs in two different external electric fields: (a) 13 kV/cm and (b) 17 kV/cm. The blue subbands are the designed lasing levels and the red ones are the injection levels. The layer thicknesses are **3.95**/7.99/**2.16**/9.02/**3.19**/6.86/**3.76**/*14.38* (nm). The widest well is doped at a sheet density of $n = 2.95 \times 10^{10}$ cm^{-2}.

This combination of injection with the emission process also overcomes the critical injection barrier thickness in the RT injection scheme, and achieves a wider dynamic range for the operating current density. In the RT injection design, the dynamic range of the operating current density is related to the emission energy of the QCLs because the resonant condition

for lasing corresponds to the subband alignment from $l_{2',1'}$–l_4 to $l_{2',1'}$–l_5 [8]. The radiative energy at low frequencies (~8 meV for 2 THz) is similar to the typical energy broadening of the subbands, which is in the range of a few meV. This causes difficulties for selectively and correctly injecting carriers from $l_{2',1'}$ to l_5. A wider injection barrier can maintain superior injection selectivity and restrain the $l_{2',1'}$–l_4 leakage current, but also makes the injection transport incoherent and inefficient [22, 23], and reduces the strength of the emission oscillator. The realization of large population inversion (optical gain) and injection current are somehow mutually exclusive in design utilizing the RT injection scheme. This means the optimization of the injection barrier thickness is critical during the design of the structure [24]. We optimize the 2.16 nm thickness of injection barriers to give the lager leakage than the injection, and cannot achieve the required lasing condition at this electric field with simplified three-level band diagram. This injection barrier thickness is also considered for the lasing conditions in our simplified three-level system with higher external electric fields.

When we replace the injection process by a scattering process, as shown in **Figure 1(b)**, the injection from $l_{2',1'}$ to l_5 is not directly related to the RT process. These two levels are energetically separate. The RT current is not limited by the thickness of the injection barrier, and we have a wider optimization space for thinning the intrainjection barrier using the scheme shown in **Figure 3(b)** (the function of the intrainjection barrier is similar to that of the injection barrier in the RT injection scheme shown in **Figure 3(a)**: the current flows to the injection level $l_{2',1'}$ through this barrier by the RT process). This can maximize the resonant injection current flow across the cascade structure, achieving smooth and rapid population inversion at low frequencies. We also calculated the dependencies on the injection barrier and emission barrier thicknesses of the emission ($l_5 \geq l_4$), injection ($l_{2',1'} \geq l_5$), and leakage ($l_{2',1'} \geq l_4$) between the subbands. This data is used to optimize the optical gain (emission) and to smooth the injection current at 17 kV/cm (region 2 in **Figure 2**) using the indirect injection scheme in the simplified four-level band system. The dynamic range of the operating current density, as shown in **Figure 3(b)**, is also not directly limited by the subband alignment between $l_{2',1'}$ and l_4 to l_5. Carrier injection from $l_{2',1'}$ to l_5 by the LO phonon scattering process has greater tolerance to the electric field and thermal perturbations. It provides a wider dynamic range for the current density even at narrow radiative energy.

Here, we demonstrate 1.9 THz $Al_{0.175}Ga_{0.825}As$/GaAs QCLs with T_{max} up to 160 K, operating at temperatures much higher than the traditional empirical $h\omega/k_BT$ limitation for RT injection at low frequencies (T_{max} ~1.8 $h\omega/k_B$). The structure utilizes an indirect scattering process for injection and a high Al-content barrier in order to achieve a larger spatial separation between the wavefunctions and more diagonal THz emission. It is also easier to realize an indirect injection scheme in the THz region using the AlGaAs/GaAs material. Moreover, this design has greater tolerance to both the electric field and thermal perturbations with a smooth current flow. We estimated that this kind of combination design scheme has better selectivity relative to the correct level of injection. With careful optimization of the wavefunctions, we realized lasing at frequencies below 2 THz only. With the structure optimized in different directions, this design scheme for THz QCLs is a promising means for extending QCLs to lower frequencies and also to higher temperature operation. The further design of these indirect injection

THz QCLs is possible by the larger design freedom modulation height barrier-well active structure design, which we will describe in the next paragraph.

3. Modulation barrier-well active structure design THz QCLs

In order to design the further indirect injection THz QCLs with more design freedom in narrow energy THz frequency, which traditionally usual suffered from opposite thickness optimization. Here, we introduce the active structure design with different heights of barriers and wells. First, we present primary experimental results by arranging the recently recorded three-well resonant tunneling structure design; modulate the Al the height of barriers with the different emission barrier compositions and introduce an external thin barrier in the widest extraction/injection well. This modulation barrier THz QCL sample succeeds lasing at 3.7 THz with the maximum operation temperature of up to 145K.

Currently, the best performing designs are mainly based on the resonant phonon depopulation scheme for extraction utilizing the AlGaAs/GaAs material systems with one kind of Al barrier concentration 15%. The modulation Al composition barrier THz QCL samples are grown by solid-state MBE with multiple Al cells. The thickness and Al compositions are precisely controlled within 1% difference. Then the devices are fabricated in the Cu-Cu metal-metal waveguide by photolithograph and dry etching. The active region structure design and band diagram are shown in **Figure 4**.

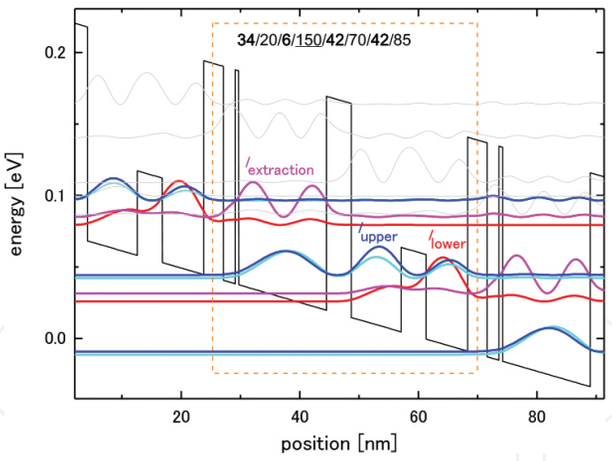

Figure 4. Band diagram of our modulation barrier THz QCLs in this paper. Based on the three-well resonant tunneling design and arranged with one external thin barrier and lower emission barrier.

First, we follow the three-well resonant tunneling injection design [7], achieve diagonal emission and increase the spatial separation between upper and lower lasing levels in order to reduce the parasitic injection leakage comes from nonradiative thermally activated longitudinal phonon scattering at high temperature operation. At the widest extraction/injection well, we expected to add an external thin and high layer in order to improve extraction by interface roughness (IR) scattering, which is one solution used in mid-infrared QCL design

[25]. The simulated Al composition of this external barrier with an amount of IR scattering, oscillator strength between the extraction/injection level (l_{ext}) to upper lasing level (l_{upper}) and the lower lasing level (l_{lower}) is shown in **Figure 5**. The extraction from the l_{lower} to l_{ext} can induce by the fast elastic IR scattering comes from this thin external barrier with the increase of barrier height; the extraction/injection efficiency can be improved by increasing the barrier height, as shown at the circle point in **Figure 5**. The related oscillator strength of l_{ext} to l_{upper} and l_{lower} (square and triangle points) is decrease and increase with the increase of the barrier height inversely. It means that the wavefuctions of l_{ext} are more localized in the extraction/injection well; the plastic leakage from the l_{upper} to l_{ext} can be reduced. In the same time, maintain the strong extraction from l_{lower}. Finally, the injection selectively and efficiency can be improved in the resonant tunneling scattering design. But the too thin layer causes the difficulty to the growth thickness control.

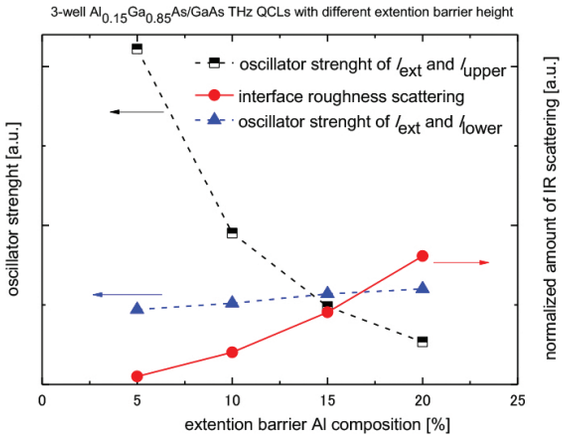

Figure 5. Simulation of external barrier Al composition with the amount of IR scattering, oscillator strength between the extraction/injection level (l_{ext}) to upper lasing level (l_{upper}) and the lower lasing level (l_{lower}).

For the further design, we also would like to increase all the barrier compositions, so here we first keep this thin barrier composition the same with others barriers at 15%. The lower emission barrier between two emission wells is modulated in order to reduce the nonradiative IR scattering at the emission layers. The Al composition of the emission barrier with the amount of IR scattering and oscillator strength between two lasing levels (l_{upper}, l_{lower}) is calculated as shown in **Figure 6**. The amount of IR scattering is proportional to the square of barrier height (Al composition 7.5% barrier in **Figure 4**). Reduction of barrier height is an efficient way to exclude this nonradiative scattering in the emission region. The utilization of a lower emission barrier height of 7.5% is to keep the oscillator strength same as the original design and reduces the IR scattering. The design **34**$_{(0.15)}$/20/**6**$_{(0.15)}$/150/**42**$_{(0.15)}$/70/**42**$_{(0.075)}$/85 **Al$_x$Ga$_{1-x}$As$_{(y)}$**/GaAs modulation THz QCLs are measured by the cryogenic cryostat with the Si-bolometer and FT-IR system in pulse mode. The maximum operation temperature (T_{max}) is up to 112 K with a threshold current density of 0.85 kA/cm^2 and wide operation current density dynamics range about 1 kA/cm^2. The 3.7 THz peak is operated up to the T_{max} of this device. This frequency is consistent with the design energy separation of 15.5 meV between two lasing levels under designed operation electric fields of 12.6 kV/cm. But at low operation temperature below 90

K, one more unexpected peak also estimates at around 3.4 THz. This multiple peaks can be explained by the transition from both $l_{upper(1,2)}$, as shown in **Figure 4**. The similar wavefunctions and oscillator strength to l_{lower} ($f_{upper1-->lower} = 0.26$ and $f_{upper2-->lower} = 0.23$) with an energy separation of about 1.2 meV (0.3 THz) of two upper lasing levels during the designed electric field. This energy separation is consistent with the frequency difference between two peaks. The wider operation current density dynamics range also can be explained by the combination of two lasing *I-L* characteristics of maniple lasing. These might come from the structure not well optimized near the emission levels and reduced the total injection efficiency to the designed upper lasing level and resulting in the lower temperature performance as we expected for this primary modulation barrier THz QCLs.

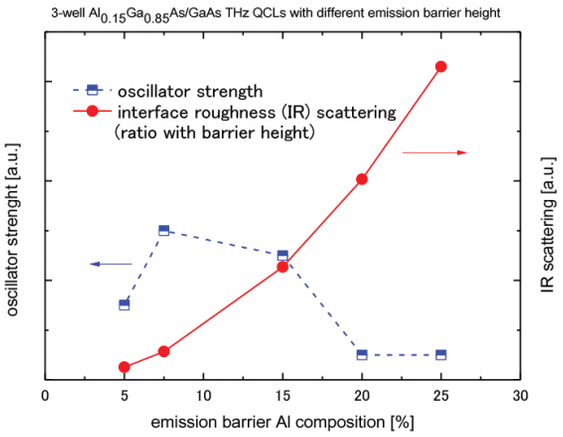

Figure 6. Simulation of emission barrier Al composition with the amount of IR scattering, oscillator strength between two lasing levels (l_{upper}, l_{lower}).

We utilize the lower emission barrier to reduce the IR scattering at the emission region, add an external thin barrier to improve the injection efficiency and reduce plastic leakage current from l_{upper} to l_{ext}. We demonstrate the lasing of this kind of modulation barrier design structure but still show the poor temperature performance lower than we expected. The active structure from this approach, as the result, is similar to the other theoretical design of THz QCLs with different barrier height [12]. On the basis of initially experimental results, we further optimize the thickness of emission barriers in order to deaden the multiple lasing and improve the temperature operation at the designed 3.7 THz. Then obtained the expected 3.7 THz operation only with the same threshold current density, and finally give T_{max} to 145 K. The future structures optimization and utilize the indirect injection scheme combine with high Al composition design in injection layers with low Al composition in emission layers. We expect the realization of thermoelectric cooling temperature operation THz QCLs.

4. Relatively compact-size potable condenser type THz source by QCLs

After introduce the recent fabricated THz QCLs toward high temperature operation at low frequency (<2 THz) and the 3–4 THz region. For THz applications, the output power is more

http://dx.doi.org/10.5772/65351

critical than the operation temperature. Even the recent devices cannot operate at the room temperature. Utilizing some kinds of cryogenic systems, it is still possible to achieve the relatively compact size potable THz application by THz QCLs. Here, we introduce the liquid nitrogen Dewar condenser to combine the fabricated THz QCLs as mentioned above. The size of Dewar is 14 cm^2 with 28 cm high without the outside external power supply (**Figure 7(a)**), the QCL sample array (**Figure 7(c)**) is fixed under vacuum conditions with cooling holder direct cooled by heat conduction from LN_2. The QCL samples are combined with hyperhemispherical Si lens in front of operated mesa and an adjustable inside parabolic mirror in order to focus the output of THz QCLs (**Figure 7(d)**) and give the near collimated THz wave outside the measurement Tsurupica windows from the widely diverged MMW QCLs.

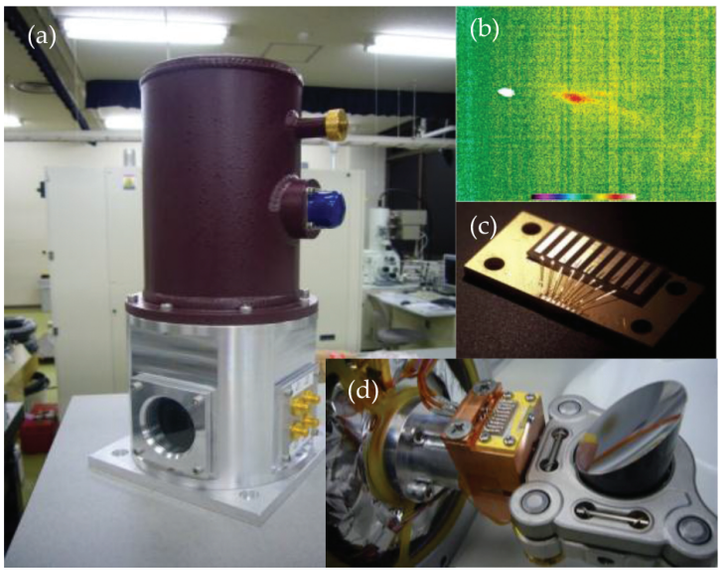

Figure 7. (a) The photograph of the Dewar condenser. (b) Far-field pattern of the Dewar condenser measured using NEC THz camera IR/V-T0831. (c) The photograph of fabricated THz QCL array with 9 mesas. (d) The fixed QCL array with hyperhemispherical Si lens and an adjustable parabolic mirror inside.

In our case, without the hyperhemispherical Si lens, the far-field pattern angle of MMW QCLs is about 40°. If coupled with the Si lens, it is possible to adjust the maximum output near 0°. This is very helpful for the adjusting the THz wave from the small size measurement window and use for real applications. The far-field pattern is also shown in **Figure 7(b)**, which measured using the NEC THz camera IR/V-T0831. The adjustment of the position of Si lens is also quite important for the increasing the output power, with and without the Si lens, the measured out power can be increased about 2.5–3 times. The active region design is based on the four well-resonant tunneling injection LO depopulation scheme with the variable barrier height modulation active structure THz QCLs as discussed above, which originally toward the high temperature operation. The waveguides also use the high temperature operation MMW. The output peak power is 0.1 mW with a duty cycle of 0.02% (1 kHz repeated frequency with 200 ns pulse width). When the duty cycle increases to 5% (10 kHz repeated frequency with 5 μs pulse width), the device gives the 37 μW average power with >1 mW peak power. The changes in duty cycle by changing the repeated input pulse frequency and pulse width are related to

the peak output power of THz QCLs when the pulse width is below 1 μs. The too short pulse did not supply the enough input energy for devices. The peak power is become stable when the input pulse is larger than 1 μs. But the average power can be increased continuously with the increasing duty cycle.

Recently, our stable pulse generator (AVTECH AVO-6HZ-B) with impedance match can only operate up to 5%. The device can possibly operate at higher duty cycle with larger average output power. But when the duty cycle increases, the heat generated from the device is quite large during the operation, comparing with the measurement condition 0.02%, even with the use of continuous flow liquid helium cryostat. The device heat sink temperature is increased up to 30 K during the operation. For the Dewar case, the duty cycle is larger than 1%. The recent contact electrode by indium ball and 0.07 mm-thin cupper wire for electric connection is easy to be melted. It causes the difficulty for stable CW operation. The measurement spectrum and the stable operation of current density-voltage, current density-light output characteristics direct from the Dewar condenser, are shown in the inset of **Figure 8**. We can find that the Dewar gives the clear single color 3.8 THz lasing spectrum, stable milliwatt order peak power and microwatts order average power. The maximum peak power is 3.1 mW and maximum average power is 6.2 μW under recent Dewar setting conditions.

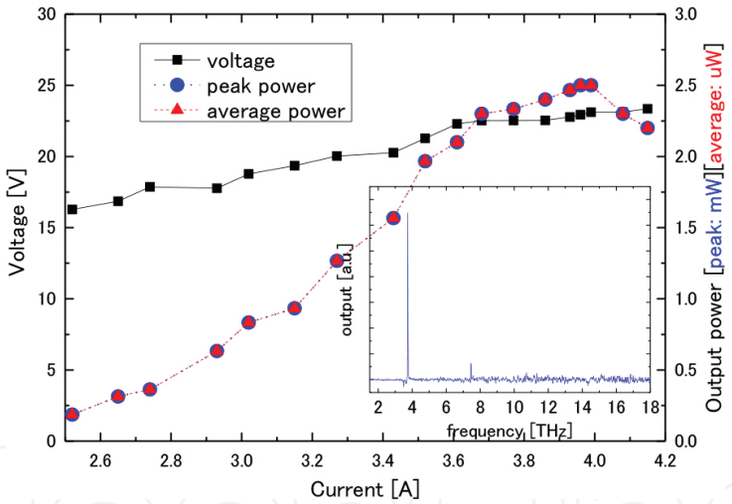

Figure 8. The measurement lasing spectrum and the stable operation of current density-voltage, current density-light output characteristics direct from the Dewar condenser.

For the CW operation with milliwatt average output power, the improvement for the recent Dewar system mainly obtained by two directions: first is the THz QCL device, recently the QCLs used in this condenser are toward the high temperature operation MMW QCLs with narrow ridge width and small mesa size. The output performance of THz QCLs generally decreases when the operation temperature is above 100 K. Upon cooling with the LN_2, the performance do not dramatically change to a large extent under low temperature conditions. The few tens K temperature operation is not important for this Dewar setting. The device fabrication move to the larger mesa size SI-SP waveguide can improve the output performance with the better far-field pattern. It is suitable for the high output 77 K Dewar condenser with

http://dx.doi.org/10.5772/65351

the easier optical aliment in applications. Second direction is the improvement and consideration of cooling efficiency of the Dewar condenser. The recent operation duty cycle is limited by the wire connection and the electrode of the mounted sample holder not by the device itself. If we can reduce the temporary heat increase with large duty cycle by wide size heat conduction and good thermal conductivity, it is possible to improve the operation duty cycle of the Dewar condenser.

On the basis of the first direction, we introduce the recent fabricated modulation active structure THz QCL cooling and setting with the active structure design by more vertical emission and large current injection. This way we achieve the large output THz QCLs with a peak power of 250 mW and an average power of 2.2 mW under the condition of duty cycle 1%. L-I-V characteristics, lasing spectrum, and far-field pattern measured using THz camera are shown in **Figure 9**. The LN_2 Dewar condense demonstrated as a robust compact size THz source unit with stable milliwatt order peak power and microwatts order average power operation by THz QCLs. And the large output power devices without high temperature operation (>100 K) also show the potential for the more powerful THz source unit toward the target of CW operation with milliwatt average output power. For further improvement of Dewar condenser, we replace the recent fabrication by SI-SP waveguide with large mesa size and high output power active region design, increase the current duty cycle limitation comes from the power supply, cooling efficiency of connect wire and electrode.

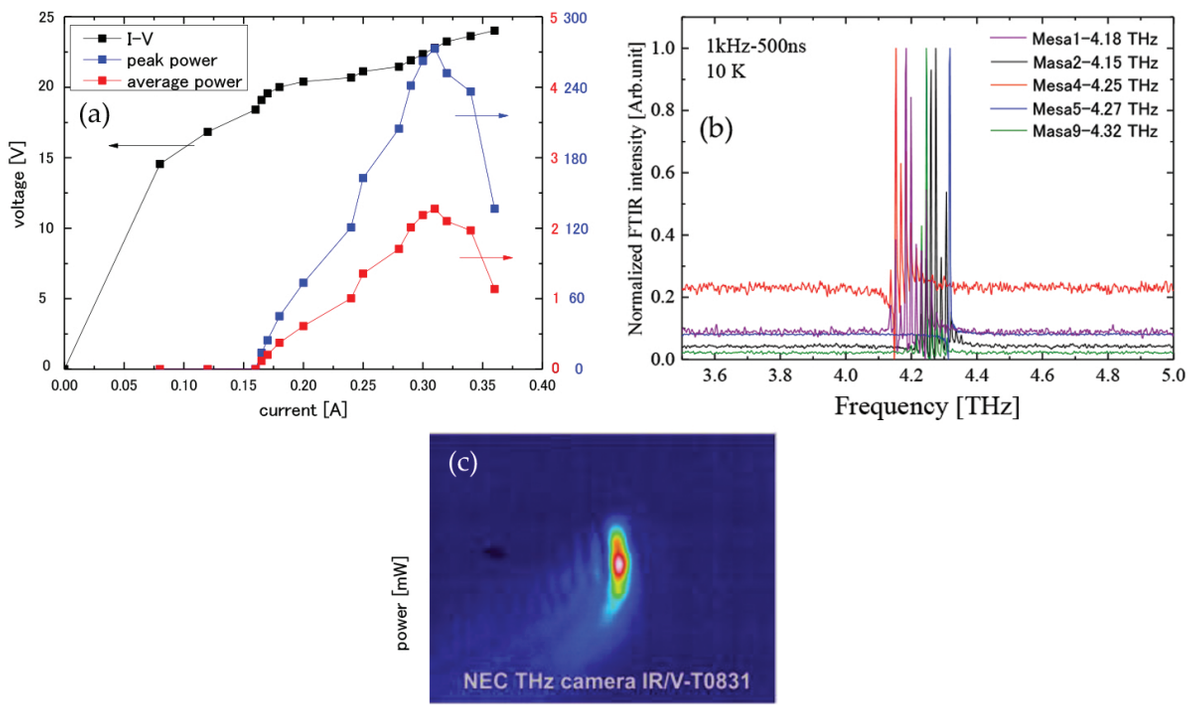

Figure 9. The measurement of (a) current density-voltage, current density-light output characteristics, (b) lasing spectrum, and (c) far field pattern of large output THz QCLs.

Here, we discuss the design and fabrication of THz QCLs toward the high temperature and large average output power operations for the real THz applications with the relatively

compact portable size cryogenic cooling systems. We also describe the temperature performance parameters of THz QCLs, introduce the results of an indirect injection design scheme in the THz region and modulation height active structure design with different barriers and wells for further design direction. The recent fabricated THz QCLs are combined with the liquid nitrogen cooling Dewar condenser to demonstrate the relatively compact potable THz source unit by QCLs. The different injection schemes in THz and barrier-well height design in the active region introduce one of the directions for the further high temperature and large output power operation of THz QCLs for real applications.

Author details

Tsung-Tse Lin

Address all correspondence to: ttlin@riken.jp

RIKEN Center for Advanced Photonics, Terahertz Quantum Device Research Team, Sendai, Japan

References

[1] T. K.-Ostmann and T. Nagatsuma: J. Infrared. Milliw. TE. 32 (2011) 143.

[2] J. Faist, F. Capasso, D. L. Sivco, C. Sirtori, A. L. Hutchinson, and A. Y. Cho: Science 264 (1994) 553.

[3] R. Köhler, A. Tredicucci, F. Beltram, H. E. Beere, E. H. Linfield, A. G. Davies, D. A. Ritchie, R. C. Iotti, and F. Capasso: Nature 417 (2002) 156.

[4] C. Walther, M. Fischer, G. Scalari, R. Terazzi, N. Hoyler, and J. Faist: Appl. Phys. Lett. 91 (2007) 131122.

[5] C. W. I. Chan, Q. Hu, and J. L. Reno: Appl. Phys. Lett. 101 (2012) 151108.

[6] L. Li, L. Chen, J. Zhu, J. Freeman, P. Dean, A. Valavanis, A.G. Davies, and E. H. Linfield: Electron. Lett. 50 (2014) 309.

[7] S. Fathololoumi, E. Dupont, C. W. I. Chan, Z.R. Wasilewski, S.R. Laframboise, D. Ban, A. M'aty'as, C. Jirauschek, Q. Hu, and H. C. Liu, Opt. Express 20 (2012) 3866.

[8] S. Kumar, C. W. I. Chan, Q. Hu, and J. L. Reno: Nat. Phys. 7 (2011) 166.

[9] T.-T. Lin, L. Ying, and H. Hirayama: Appl. Phys. Express. 5 (2012) 012101.

[10] C. W. I. Chan, Q. Hu, and J. L. Reno: Appl. Phys. Lett. 103 (2013) 151117.

[11] G. Scalari, M. I. Amanti, M. Fischer, R. Terazzi, C. Walther, M. Beck, and J. Faist: Appl. Phys. Lett. 94 (2009) 041114.

[12] A. Matyas, R. Chashmahcharagh, I. Kovacs, P. Lugli, K. Vijayraghavan, M. A. Belkin, and C. Jirauschek: J. Appl. Phys. 111 (2012) 103106.

[13] B. S. Williams, S. Kumar, Q. Hu and J. L. Reno: Electron. Lett. 42 (2006) 89.

[14] M. Yamanishi, K. Fujita, T. Edamura, and H. Kan: Opt. Express. 16 (2008) 20748.

[15] H. Yasuda, T. Kubis, P. Vogl, N. Sekine, I. Hosako, and K. Hirakawa: Appl. Phys. Lett. 94 (2009) 151109.

[16] T. Kubis, S. R. Mehrotra, and G. Klimeck: Appl. Phys. Lett. 97 (2010) 261106.

[17] T. Liu, T. Kubis, Q. J. Wang, and G. Klimeck: Appl. Phys. Lett. 100 (2012) 122110.

[18] E. Dupont, S. Fathololoumi, Z. R. Wasilewski, G. Aers, S. R. Laframboise, M. Lindskog, S. G. Razavipour, A. Wacker, D. Ban, and H. C. Liu: J. Appl. Phys. 111 (2012) 073111.

[19] K. Fujita, M. Yamanishi, S. Furuta, K. Tanaka, T. Edamura, T. Kubis, and G. Klimeck: Opt. Express 20 (2012) 20647.

[20] S. G. Razavipour, E. Dupont, S. Fathololoumi, C. W. I. Chan, M. Lindskog, Z. R. Wasilewski, G. Aers, S. R. Laframboise, A. Wacker, Q. Hu, D. Ban, and H. C. Liu: J. Appl. Phys. 113 (2013) 203107.

[21] T.-T. Lin and H. Hirayama: Phys. Stat. Sol. C 10 (2013) 1430.

[22] C. Sirtori, F. Capasso, J. Faist, A.L. Hutchinson, D. L. Sivco, and A. Y. Cho: IEEE J. Quantum Electron 34 (1998) 1722.

[23] S. Kumar and Q.Hu: Phys. Rev. B 80 (2009) 245316.

[24] H. Callebaut and Q. Hu: J. Appl. Phys. 98 (2005) 104505.

[25] Y. Chiu, Y. Dikmelik, J. B. Kurghin, and C. Gmachl: in the 11th International Conference on Intersubband Transitions in Quantum Wells, Sardinia, Italy (2011).

IntechOpen